

# Deep learning empowered sensor fusion to improve infant movement classification

Tomas Kulvicius<sup>1,2,3,12,\*</sup>, Dajie Zhang<sup>2,4,12</sup>, Luise Poustka<sup>2</sup>, Sven Bölte<sup>5,6,7</sup>,  
Lennart Jahn<sup>1,3</sup>, Sarah Flügge<sup>1</sup>, Marc Kraft<sup>8</sup>, Markus Zweckstetter<sup>2,9,10</sup>, Karin Nielsen-Saines<sup>11</sup>,  
Florentin Wörgötter<sup>3,13</sup>, and Peter B Marschik<sup>1,2,4,5,13,\*</sup>

<sup>1</sup>Child and Adolescent Psychiatry and Psychotherapy, University Medical Center Göttingen, Leibniz ScienceCampus Primate Cognition and German Center for Child and Adolescent Health (DZKJ), Göttingen, Germany

<sup>2</sup>Department of Child and Adolescent Psychiatry, University Hospital Heidelberg, Ruprecht-Karls University of Heidelberg, Heidelberg, Germany

<sup>3</sup>Department for Computational Neuroscience, Third Institute of Physics - Biophysics, Georg-August-University of Göttingen, Göttingen, Germany

<sup>4</sup>iDN – interdisciplinary Developmental Neuroscience, Division of Phoniatics, Medical University of Graz, Graz, Austria

<sup>5</sup>Center of Neurodevelopmental Disorders (KIND), Department of Women’s and Children’s Health, Center for Psychiatry Research, Karolinska Institutet & Region Stockholm, Stockholm, Sweden

<sup>6</sup>Child and Adolescent Psychiatry, Stockholm Health Care Services, Region Stockholm, Stockholm, Sweden

<sup>7</sup>Curtin Autism Research Group, Curtin School of Allied Health, Curtin University, Perth, Australia

<sup>8</sup>Department of Medical Engineering, Technical University Berlin, Berlin, Germany

<sup>9</sup>German Center for Neurodegenerative Diseases (DZNE), Göttingen, Germany

<sup>10</sup>Department for NMR-based Structural Biology, Max Planck Institute for Multidisciplinary Sciences, Göttingen, Germany

<sup>11</sup>Department of Pediatrics, David Geffen UCLA School of Medicine, Los Angeles, CA, USA

<sup>12</sup>These authors contributed equally

<sup>13</sup>These authors jointly supervised this work

\*Corresponding authors: Dr. Tomas Kulvicius, tomas.kulvicius@med.uni-goettingen.de; Prof. Peter B Marschik, peter.marschik@med.uni-heidelberg.de

## Abstract

There is a recent boom in the development of AI solutions to facilitate and enhance diagnostic procedures for established clinical tools. To assess the integrity of the developing nervous system, the Prechtl general movement assessment (GMA) is recognized for its clinical value in diagnosing neurological impairments in early infancy. GMA has been increasingly augmented through machine learning approaches intending to scale-up its application, circumvent costs in the training of human assessors and further standardize classification of spontaneous motor patterns. Available deep learning tools, all of which are based on single sensor modalities, are however still considerably inferior to that of well-trained human assessors. These approaches are hardly comparable as all models are designed, trained and evaluated on proprietary/silo-data sets. With this study we propose a sensor fusion approach for assessing fidgety movements (FMs) comparing three different sensor modalities (pressure, inertial, and visual sensors). Various combinations and two sensor fusion approaches (late and early fusion) for infant movement classification were tested to evaluate whether a multi-sensor system outperforms single modality assessments. The performance of the three-sensor fusion (classification accuracy of 94.5%) was significantly higher than that of any single modality evaluated, suggesting the sensor fusion approach is a promising avenue for automated classification of infant motor patterns. The development of a robust sensor fusion system may significantly enhance AI-based early recognition of neurofunctions, ultimately facilitating automated early detection of neurodevelopmental conditions.

# 1 Introduction

In recent years, we have seen a boom in the development of automated solutions for the Prechtl general movements assessment (GMA). These efforts utilize AI methods in the attempt to improve classic clinical assessments by removing potential subjectivity in implementation and reducing the long term costs associated with training and qualifying human experts [1, 2, 3, 4, 5, 6, 7]. The original GMA, introduced in the late 1990s, is a validated diagnostic tool based on a human gestalt appraisal of infants’ endogenously generated motor functions to detect neurological impairments within the first few months of life [8]. Compared to other diagnostic tools such as MRI, GMA can be implemented by experts within minutes without the need of anyone touching the infant, while delivering unbeatable diagnostic accuracy [8, 9]. Recent automated GMA attempts mainly focus on identifying a single medical condition by tracking and classifying a fraction of motor patterns which the original GMA evaluates. We are still a long way away for the proposed AI methodology to approach the utility of the original GMA, both in regards to technology and diagnostic scope.

Different sensor modalities for AI-driven GMA have been developed, each with its own strengths and limitations [10, 1, 2, 3, 4, 5, 6, 7]. Most of these automated approaches were developed based on visual data (with RGB/RGB-D imaging sensors; [11, 12, 13, 7, 14, 15, 16, 17, 18, 19, 20, 21]), which is also the data source of ‘original GMA’. Methods using marker-based body tracking [22] or wearable sensors, e.g., inertial measurement units (IMUs) [23, 24, 25, 26, 27, 28, 29, 30], encouraged by their success in adult motion tracking, were also proposed for use in infants. Pressure sensing devices have been employed in the assessment of general movements [5, 31, 32, 10], since they are non-intrusive and easy to use, hence being particularly suitable for clinical practice. At present, the development of automated GMA approaches is still in its infancy, mostly based on small datasets, with minimal data-sharing or pooling, and targeting only a fraction or a specific aspect of the tasks involved in the standard GMA. Most AI methods focus understandably on the classification of fidgety movements (e.g., present or absent, typical or atypical; [7, 10, 18, 1, 2, 3, 4, 5, 6], a general movements pattern of high diagnostic value for the early detection of neurodevelopmental integrity at around three months post-term age [8, 9, 33]. The classification performances of single modality methods, irrespective of their task specifics and different participants samples, compete with each other with an accuracy level of about 90%. This is considerably inferior to that of well-trained human assessors and the methodologies cannot be compared to each other as all models are designed, trained and evaluated on proprietary datasets [1, 2, 3, 4, 5, 6, 10, 34, 18, 7, 27, 35, 36].

Targeting a higher accuracy, we proposed a multi-sensory recording setup and sensor fusion approach for automated GMA, utilizing different combinations of video cameras, pressure sensing devices, and IMUs [37, 5, 26, 27, 35, 36]. The rationale behind the sensor fusion approach is that each motion tracking modality captures different types and dimensions of movement information (e.g., position and amplitude in space, body parts involved, force, velocity, frequency, direction, angular velocity and acceleration, etc.) which other sensors may miss or are unable to track directly. If different inputs are integrated, they may compensate and boost each other towards better performance. This approach needs to be empirically tested. To the best of our knowledge, there exists no public-accessible multi-sensory dataset of general movements, while no study has carried out any empirical comparisons of utilities of different sensing modalities, let alone their combinations, for analyzing infant motor functions and enhancing classification accuracy.

To fill in this knowledge gap, we present a labeled and fully synchronized multi-sensory dataset of infant movements. With this dataset, we develop a sensor fusion approach and undertake a deep learning empowered comparison of three different sensor modalities, pressure, inertial, and visual sensors and their various combinations for movement classification to evaluate if such a system outperforms single modality assessments.

We perform classification experiments using convolutional neural network (CNN) architectures and compare two different sensor fusion approaches, early (using one neural network) vs. late (combining outputs of multiple neural networks) sensor fusion to address three research questions: (1) Do performances of different sensor modalities differ from each other for the same task (i.e., tracking and classifying fidgety vs. non-fidgety movements)? (2) Does sensor fusion outperform single modality assessments and lead to higher accuracy in infant movement classification? (3) Is a sensor fusion approach with non-intrusive sensors sufficient for accurate movement tracking and classification?

## 2 Methods

### 2.1 Method overview

A flow diagram of the study pipeline is shown in Figure 1. In this study we used data collected and pre-processed by our research group at iDN’s BRAINtegrity lab, Medical University of Graz, Austria, and Systemic Ethology and Developmental Science Labs, University Medical Center Göttingen and University of Heidelberg, Germany [18, 35]. We collected and segmented 19451 data units from 51 biweekly assessed participants ([18, 10]; for details see section 2.2). The study aimed to analyze the ontogeny of human behavior and typical cross-domain development during the first months of human life [35]. The project was approved by the Institutional Review Boards of the Medical University of Graz, Austria (27-476ex14/15) and the University Medical Center Göttingen, Germany (20/9/19).

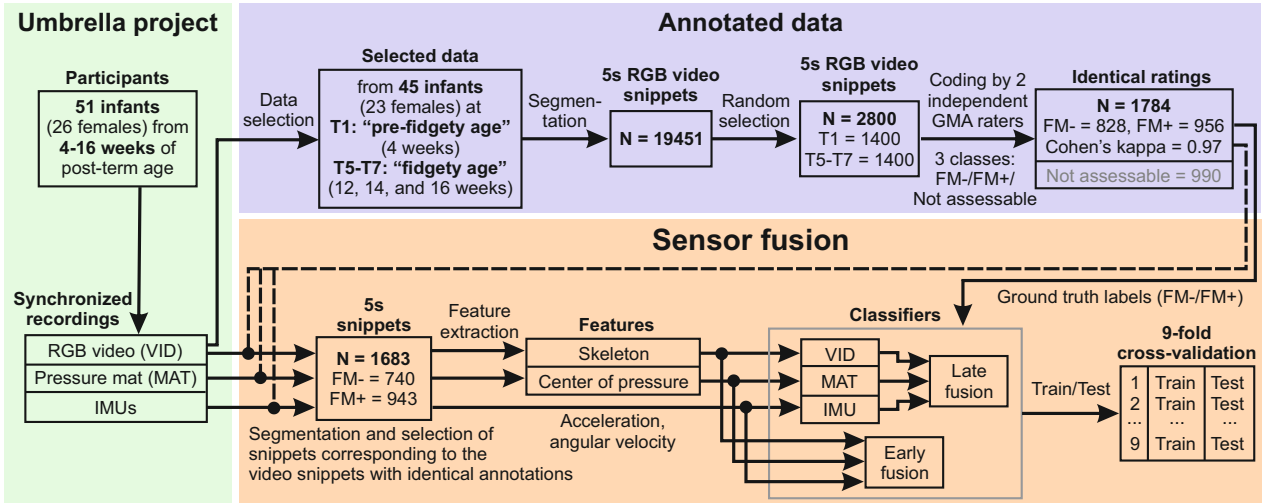


Figure 1: Flow diagram of the study pipeline. N corresponds to the number of snippets (5 s data units) in each step. T1-T7 correspond to seven recording sessions in biweekly intervals, starting at 4 weeks post-term age. FM- and FM+ corresponds to the absence and presence of fidgety movements, respectively. VID – video data, MAT – pressure mat data, IMU – inertial measurement unit data.

In this study, we adopted movement data captured by three different sensor modalities: a 2D RGB camera, a pressure sensing mat, and six inertial measurement units (IMUs). For movement classification based on video data, we used skeleton features as presented in prior studies [18, 34]. For movement classification based on pressure mat data, we used center of pressure (CoP) features as presented in a prior study [10]. Data from the IMUs and IMU-based classification are reported here for the first time. Based on our previous work, for the movement classification we used convolutional neural network (CNN) architectures, which is superior for the current task compared to other classification methods such as multi-layer perceptron (MLP), support vector machine (SVM) and long short-term memory (LSTM) network [10].

We compared performance of movement classification when (a) using single sensor modalities, (b) using two-sensor fusion (combinations of two different sensor modalities), and (c) using a three-sensor fusion model (a combination of all sensor modalities). For the evaluation and comparison of these approaches, we used a 9-fold cross-validation procedure where test sets contained data only from infants not included in the training sets.

In the following sections we provide details on data acquisition and processing, movement analysis and classification.

## 2.2 Dataset

### 2.2.1 Participants

51 infants born between 2015 and 2017 from monolingual German speaking families were sampled. All parents of the participating infants provided written informed consent to study participation and

publication of depersonalized data. Infant inclusion criteria were: uneventful pregnancy, uneventful delivery at term age ( $> 37$  weeks of gestation), singleton birth, appropriate birth weight, uneventful neonatal period, inconspicuous hearing and visual development. All parents completed high-school or higher level of education and had no record of alcohol or substance abuse.

We post-hoc excluded one infant due to a rare genetic disorder diagnosed at three years of age. Another five infants were excluded due to lack of full recordings within the required age periods. Thus, the final sample for this study consisted of 45 infants (23 females).

## 2.2.2 Multi-modal movement recordings

We recorded infant movements from 4 to 16 weeks of post-term age in biweekly intervals at 7 succeeding sessions in a standardized laboratory setting. Data recording procedure followed the standard GMA guidelines [38]. Post-term ages at the seven sessions were T1:  $28 \pm 2$  days, T2:  $42 \pm 2$  days, T3:  $56 \pm 2$  days, T4:  $70 \pm 2$  days, T5:  $84 \pm 2$  days, T6:  $98 \pm 2$  days, and T7:  $112 \pm 2$  days corrected age.

According to the GMA manual [38], 5 to 8 weeks of post-term age mark a period (periods T2 and T3) of transitional movements which is considered a “grey”-zone between the writhing and the fidgety movement (FM) periods, which is not ideal for assessing infant general movements. FMs are most pronounced in typically developing infants from 12 weeks of post-term age onwards (corresponding to the T5-T7 periods) [38]. Therefore, to analyze infant general movements, recordings from T1 as the “pre-fidgety period” and T5-T7 as the “fidgety period” were used. Each session, infants were dressed with specifically designed body-suits (see Figure 2c) and placed in a supine position in a standard crib by the parent. We recorded infant movements using an RGB camera, a pressure sensing mat, and six inertial measurement units (IMU). All sensor recordings were synchronized [35].

For video recordings, we used a standard HD camcorder with a resolution of  $1920 \times 1080$  pixels, and a frame rate of 50 frames per second [18]. The pressure data was acquired using a Conformat pressure sensing mat (Tekscan, Inc., South Boston, Massachusetts, USA [39]). This pressure sensing mat contains 1024 pressure sensors arranged in a  $32 \times 32$  grid array on an area of  $471.4 \times 471.4 \text{ mm}^2$ . The mat was laid on the crib mattress and covered by a cotton sheet. The pressure mat produced pressure image frames (see Figure 2b) with a resolution of  $32 \times 32$  pixels, and  $100 \text{ Hz}$  sampling rate [10]. To capture infant motion using wearable sensors, six wireless Xsense MTw Awinda IMUs [40] were applied. Each IMU sensor contains a 3-axis accelerometer and a 3-axis gyrometer, which measure acceleration and angular velocity in  $X$ ,  $Y$ , and  $Z$  directions with a sampling rate of  $60 \text{ Hz}$ . Four IMU sensors were each fed into a designated pocket of a customized body-suit and attached to the infant’s shoulders and the outsides of the hips to assess proximal movement features. The other two IMUs were each put into a sock and attached to the soles of the infant’s feet for distal features in the lower extremities (for sensor locations see Figure 2c).

## 2.2.3 Movement annotations

For this study, to train and test classifiers, we used human-annotation data (see Figure 1). Annotations were performed on video recordings, which were synchronized with IMU sensors and the pressure sensor such that the same labels were used for all sensor modalities. To annotate video data, videos were first cut such that infants were overall awake and active, and not fussy. We determined the length of video snippet to be 5 seconds, as a minimum length of the video for human assessors feeling confident to judge whether the fidgety movement is present (FM+) or absent (FM-) [18, 10].

In a proof-of-concept study [18], a fraction of the total available snippets ( $N = 19451$ ) was randomly sampled ( $N = 2800$ ) and annotated by two experienced GMA assessors: 1400 from T1, the pre-fidgety period, and 1400 from T5-T7, the fidgety period (see Figure 1). Both assessors, blinded in regards to infant ages, evaluated each of the 2800 randomly ordered snippets (5 s long) independently, labeling each snippet as “FM+”, “FM-”, or “not assessable” (i.e., in case the infant was fussy, crying, drowsy, hiccuping, yawning, refluxing, over-excited, self-soothing, or distracted for the respective 5 s, all of which can distort an infant’s movement pattern rendering the recording inadequate for GMA [38, 8]).

Cohen’s kappa for the interrater agreement of the two assessors for classes FM+ and FM- was  $\kappa = 0.97$ , whereas the intrarater agreement by re-rating 10% randomly selected snippets was  $\kappa = 0.85$  for assessor 1, and  $\kappa = 0.95$  for assessor 2. Snippets with non-matching FM+/FM- labels between

two assessors ( $N = 26$ ) and the ones labeled as “not assessable” by either assessor ( $N = 990$ ) were excluded for further analysis. Thus, remaining 1784 video snippets were labeled identically by both assessors as either FM+ ( $N = 956$ ) or FM- ( $N = 828$ ). Out of the 1784 video snippets, 101 had no corresponding synchronized IMU and/or pressure mat data (due to synchronization issues), therefore, in this study, for the classification experiments 1683 (943 FM+ and 740 FM-) snippets were used.

## 2.3 Data pre-processing and feature extraction

### 2.3.1 Video data

For video-based movement classification, we used body key points as features (see Figure 2a; [18, 34]). In this study, we extracted body key points using the state-of-the-art pose estimation framework ViTPose [41], which is more accurate than OpenPose [42, 43] that we used in our previous studies [18, 34]. ViTPose extracts 17 body key points as shown in Figure 2a including key points on both ears (not shown). We excluded the two ear key points since three head key points (nose and eyes) are sufficient to determine position and orientation of the head. Thus, 15 key points were then used throughout for analyses. Given a video snippet length of 5 s, and frame rate of 50 Hz, we obtained 250 frames per video snippet with 15 key points per frame. We denoted position values for  $X$  and  $Y$  coordinates of the key points as  $x^p$  and  $y^p$ .

Several pre-processing steps were performed such as detection and removing of outliers, smoothing, centering, rotation and scaling of the skeleton key points, and normalization of position and velocity values (for details please see Supplementary Section 1).

In addition to the positions of the key points ( $x_f^{pk}, x_f^{pk}$ ), we also used their velocities ( $x_f^{vk}, x_f^{vk}$ ). After pre-processing, the feature matrix of size  $250 \times 60$  was generated.

Note that we also tried to use accelerations of the key points, however, preliminary analysis showed that including accelerations did not improve classification accuracy (see Supplementary Figure 1). Therefore, we did not include accelerations for further analysis.

### 2.3.2 Pressure mat data

The pre-processing and feature extraction procedure of the pressure mat data is shown in Figure 2b. As reported above, we used synchronized 5 s snippets corresponding to the video snippets which hence bear the same labels (FM+/FM-). Given a sampling rate of 100 Hz and the sensor grid resolution of  $32 \times 32$  sensors, resulting in 500 frames per snippet, and 1024 pressure values per frame. As features we used center of pressure (CoP) coordinates  $x^{t/b}, y^{t/b}$ , and average pressure value  $p^{t/b}$  of the top and bottom areas [10] as shown in Figure 2b (for details please see Supplementary Section 2). Finally, the feature matrix of size  $500 \times 6$  was generated.

Note that in addition to  $x^{t/b}, y^{t/b}$ , and  $p^{t/b}$  features we also tried to use their first derivatives, however, preliminary analysis showed that including derivatives as additional features did not improve classification accuracy (see Supplementary Figure 2). Therefore, we did not include derivatives for further analysis.

### 2.3.3 Inertial measurement unit data

Similar to the pressure mat data, we used synchronized 5 s snippets corresponding to the video snippets. Given an IMU sampling rate of 60 Hz, this led to 300 frames per snippet. For each IMU sensor, we obtained three accelerometer values and three gyrometer values (for each coordinate  $X, Y$ , and  $Z$ ), thus, in total 36 values per frame (see Figure 2c). We denoted accelerometer and gyrometer values as  $x^a, y^a, z^a$ , and  $x^g, y^g, z^g$ , respectively. These values, after pre-processing (see Supplementary Section 3), were then directly used as features. After pre-processing, the feature matrix of size  $300 \times 36$  was generated.

## 2.4 Neural network architectures

In this study we were dealing with a binary classification task where we classified fidgety movements (FM+) vs. non-fidgety movements (FM-). For the comparison of classification performance using different sensor modalities, we used convolutional neural network (CNN) architectures with three convolutional layers (Conv) and one fully connected (FC) layer (see Figure 3a). Each convolutional

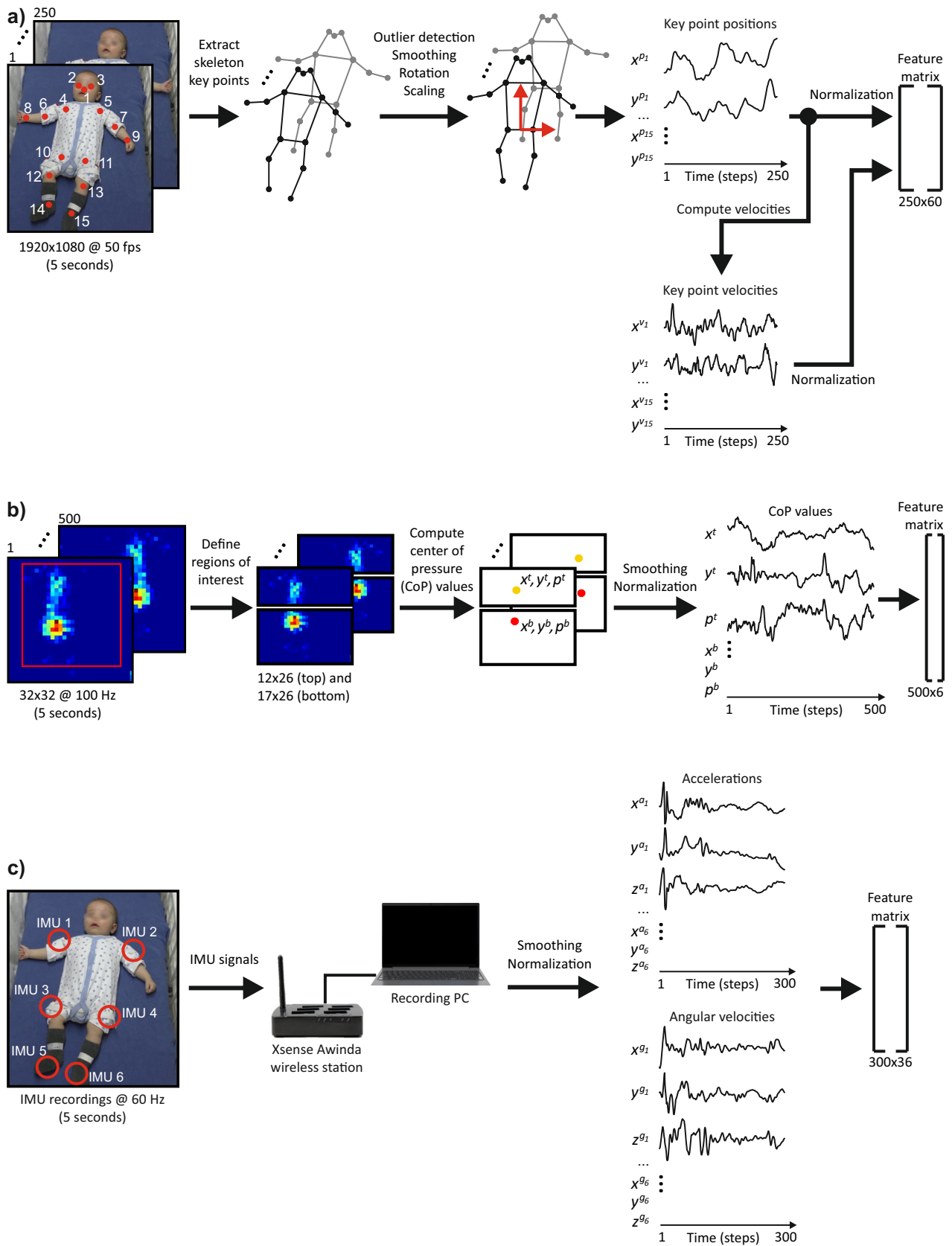


Figure 2: Flow diagrams of the feature extraction procedures for three sensor modalities: **a)** video data, **b)** pressure mat data, and **c)** IMU sensor data.

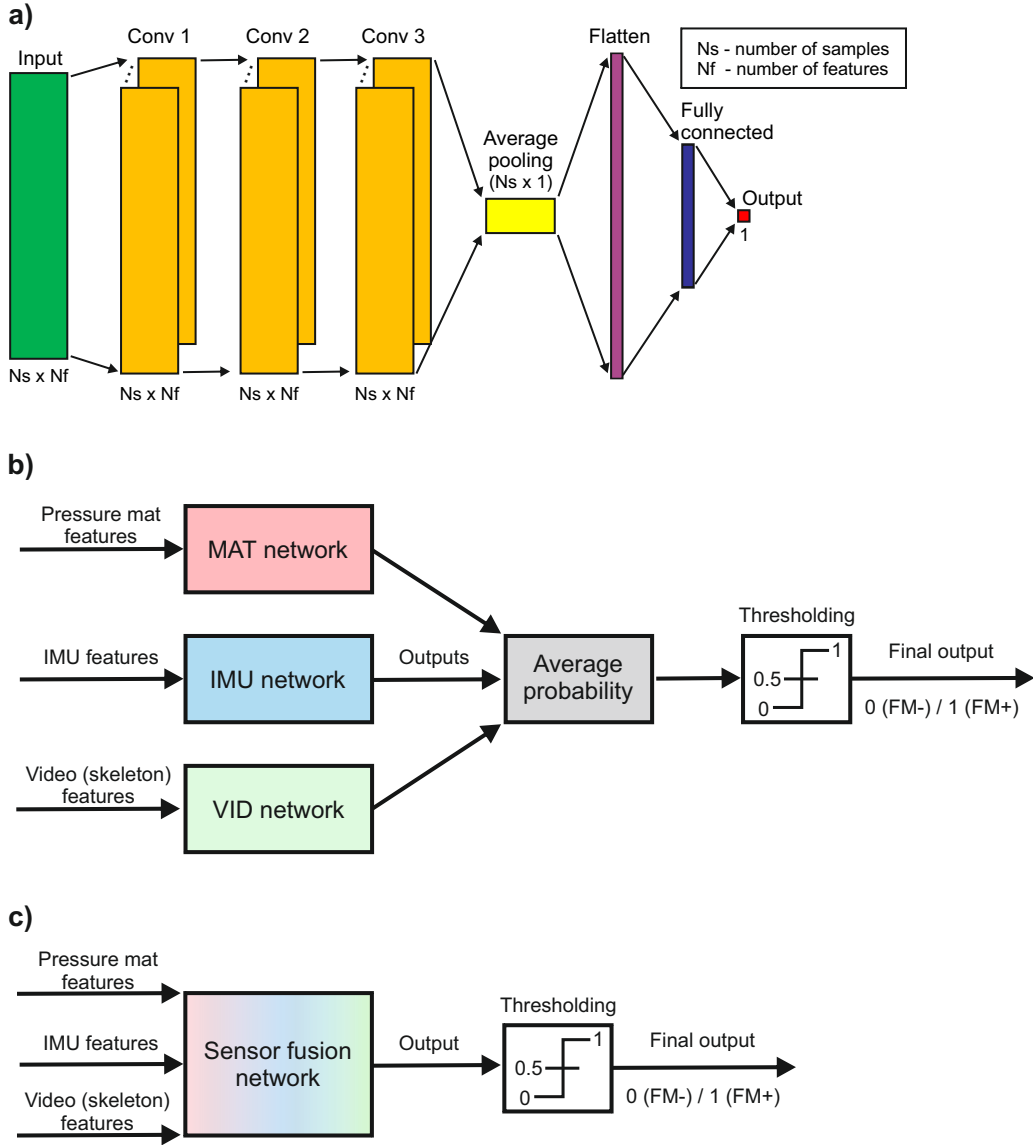


Figure 3: Classification models. **a)** Schematic diagram of the convolutional neural network (CNN) architecture. Hyperparameters for different sensor modalities are specified in Supplementary Tables 2 and 3). **b, c)** Schematic diagrams for two sensor fusion approaches: combination of three networks trained using single sensor modalities – late sensor fusion (b), and one network trained using all sensor modalities – early sensor fusion (c).

(Conv) and fully connected (FC) layer was followed by a batch normalization layer and a drop-out layer (20%). ReLU activation functions were used in the Conv and FC layers, whereas in the output layer a linear activation function was used.

To train neural classifiers, we used binary cross-entropy with *logit* transfer function as a loss function (therefore linear activation function in the output layer) and the Adam optimizer with the following parameters: batch size 4, learning rate = 0.001,  $\beta_1 = 0.9$ ,  $\beta_2 = 0.999$ , and  $\epsilon = 1e-07$ . To avoid model overfitting, we used a validation stop with the validation split 1/8 and patience of 10 epochs. The network architectures were implemented using TensorFlow [44] and Keras API [45].

## 2.5 Hyperparameter tuning

Hyperparameter tuning of the network architectures was performed on a separate dataset where snippets from 9 infants were used (data from these infants was not used in the 9-fold cross-validation procedure). The data was subdivided into training and validation sets. The number of snippets

used for hyperparameter tuning is given in Table 1.

We tuned hyperparameters of the network architectures for each sensor modality and the combination of all sensor modalities using a two-stage procedure. First, we tuned the number of convolutional (Conv) and fully connected (FC) layers, the number and size of kernels in the Conv layers, and the number of units in the FC layers using the Bayesian optimization. In the first stage, we explored architectures with 1, 2 or 3 Conv, and 1 or 2 FC layers. Other hyperparameters for the Bayesian optimization procedure are given in Supplementary Table 1. We ran Bayesian optimization for 1000 steps, and repeated this optimization procedure five times. We trained our networks using validation stop with a validation split of 1/5 and patience of 10 epochs. The other training parameters were the same as given in section 2.4. After the optimization procedure, we selected the 10 different best models with lowest loss scores on the validation set, and analyzed hyperparameters of these best models. In most of the cases, architectures with three Conv layers and one FC layer were obtained.

In the second stage, we performed fine tuning using grid search, where we fixed the number of Conv and FC layers (three and one, respectively) based on the results of the Bayesian optimization procedure, and only tuned the number and size of the kernels in the Conv layers and the number of units in the FC layer within the reduced hyperparameter space (see Supplementary Table 1). We repeated the grid search three times, where in each repetition we explored 4800 different hyperparameter sets. Finally, we selected 10 different best models (see Supplementary Tables 2 and 3.) with the lowest loss scores on the validation set. These models then were used for the 9-fold cross-validation procedure as explained in section 2.7.

The hyperparameter tuning was implemented and performed using KerasTuner [46].

## 2.6 Sensor fusion

We tested and compared two sensor fusion approaches. In the first approach (late fusion), we combined outputs of the networks which were trained on single sensor modalities (see Figure 3b). Each network outputs a value between 0 and 1, which corresponds to the probability  $p$  for the class FM+ and  $1 - p$  for the class FM-. To obtain the final decision, we averaged probabilities of two (combination of two sensor modalities) or three (combination of three sensor modalities) networks, and then applied threshold of 0.5 to obtain class label 0 or 1 for the FM- or FM+ class, respectively.

In the second approach (early fusion), we trained one network where we used features of all sensor modalities (see Figure 3c). For this, we down-sampled time series of the pressure mat and IMU features to 250 frames to make it consistent with a sampling rate of the video data. After re-sampling and concatenating three feature matrices (see section 2.3), we obtained the final feature matrix of size  $250 \times (6+36+60) = 250 \times 102$ . We used the same procedures for the hyperparameter tuning and training as explained in sections 2.4 and 2.5.

## 2.7 Evaluation procedure and quantification measures

For the evaluation and comparison of the classification models, we used a 9-fold cross-validation procedure where in total data from 36 infants were used. For this, we divided the dataset into nine subsets where each subset contained snippets from four different infants. For each fold, one subset was used as the test set, and the remaining eight subsets (snippets from 32 infants) were used to train the network architectures. The number of snippets in the training and test sets for each fold is given in Table 1.

In total we trained and tested 10 best models for each single sensor modality (see Supplementary Table 2) and the combination of all sensor modalities (see Supplementary Table 3). For training, we split the training set into training (7/8 of the training data) and validation (1/8 of the training data) subsets. For each fold we trained each model 20 times (with random initial conditions) and then selected the model with the lowest loss score on the validation set, which was then evaluated on the test set.

For the comparison of the classification performances, we used three common classification performance measures: *sensitivity* (true positive rate – TPR), *specificity* (true negative rate – TNR) and *balanced accuracy* – BA:

$$TPR = \frac{TP}{TP + FN}, TNR = \frac{TN}{TN + FP}, BA = \frac{TPR + TNR}{2}, \quad (1)$$

Table 1: Data split for the hyperparameter tuning and 9-fold cross-validation. Whole dataset consists of 1683 snippets (740 FM- and 943 FM+) obtained from 45 infants. 337 snippets (obtained from 9 infants) were used for the hyperparameter tuning and 1346 snippets (obtained from 36 infants) were used for the cross-validation.

Hyperparameter tuning (9 infants)						
	FM-	FM+	Total			
	148	189	337			
9-fold cross-validation (36 infants)						
Fold #	Training set (32 infants)			Test set (4 infants)		
	FM-	FM+	Total	FM-	FM+	Total
1	519	671	1190	73	83	156
2	537	666	1203	55	88	143
3	523	673	1196	69	81	150
4	524	665	1189	68	89	157
5	533	674	1207	59	80	139
6	521	668	1189	71	86	157
7	526	671	1197	66	83	149
8	530	672	1202	62	82	144
9	523	672	1195	69	82	151

where  $TP$  is the number of true positives,  $TN$  the number of true negatives,  $FP$  the number of false positives, and  $FN$  the number of false negatives.

To compare classification accuracies of the classification models, we calculated average classification performance measures (sensitivity [ $TPR$ ], specificity [ $TNR$ ], and balanced accuracy [ $BA$ ]) across nine test sets, confidence intervals of mean (CI 95%), and  $p$  values for the comparison of medians using the Wilcoxon two-sided signed-rank test. Statistical significance was set at  $p < 0.05$ .

## 3 Results

### 3.1 Classification performance using single sensor modalities

Comparison of the classification performance when using only one sensor modality is shown in Figure 4 and Tables 2 and 3. Note that here we compare results of the best models (out of 10). The results for all models are shown in Supplementary Table 4. The classification performance using pressure mat features (MAT, 82.1%) was lower than IMU (90.2%; approached significance,  $p = 0.055$ ), and significantly lower than skeleton (video-based) features (VID, 90.7%;  $p < 0.01$ ; Table 3). The performances of IMU and VID were not significantly different from each other.

The span of the classification accuracies using pressure mat sensor across nine test sets was large (CI 95% = [77.1% 87.0%]), which may imply that the current mat only worked well for fidgety movement classification for some infants, but not for the others. Classification accuracies using IMU and video sensors were stable across all test sets, with smaller confidence intervals, [87.6% 92.8%] and [88.9% 92.4%], respectively.

### 3.2 Classification performance using sensor fusion

Regarding two-sensor fusions (MAT+IMU, MAT+VID, IMU+VID), the classification accuracies were generally higher than those of the single modality (Table 2), although the differences were rarely statistically significant (Table 3). In particular, when fusing VID with IMU, the performance was significantly superior than that of MAT or IMU alone, but not compared to VID alone. When combining MAT with either IMU or VID, the performances were indeed significantly better than that of MAT alone, but not than IMU or VID alone. That is, adding the available sensor-mat to one of the other two sensors did not bring significant improvement than using the IMUs or the camera alone for the present task.

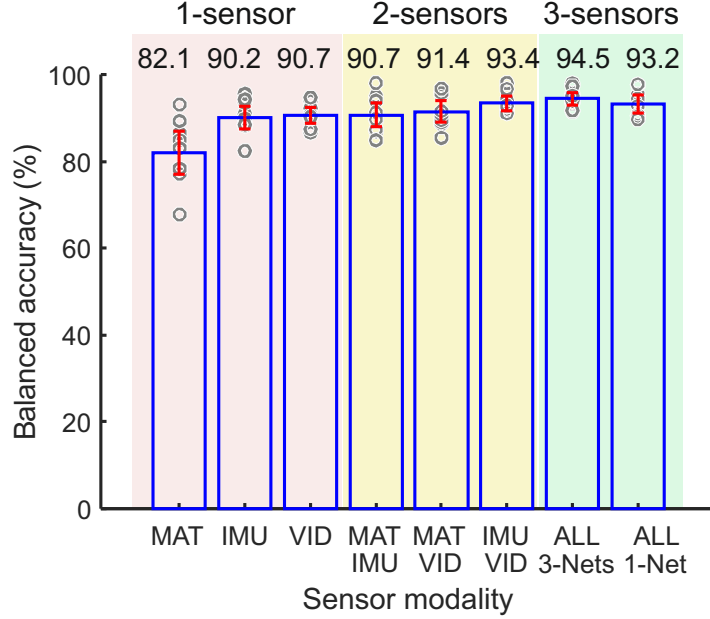


Figure 4: Comparison of classification performances of the best models of different sensor modalities on the test sets. Average balanced classification accuracy obtained from 9-fold cross-validation is shown for each case. Error bars denote confidence intervals of mean (CI 95%). Circles denote classification accuracies for each test set.

Table 2: Comparison of classification performances of the best models of different sensor modalities on the test sets. Average classification measures together with confidence intervals of mean (CI 95%) obtained from 9-fold cross-validation.

Model	Sens. (%) [ CI ]	Spec. (%) [ CI ]	BA (%) [ CI ]
Single sensor modalities (best models)			
MAT	86.17 [82.78 89.55]	77.95 [69.68 86.22]	82.06 [77.11 87.00]
IMU	92.91 [90.28 95.55]	87.52 [83.47 91.57]	90.22 [87.61 92.82]
VID	91.67 [89.80 93.55]	89.65 [85.89 93.41]	90.66 [88.91 92.41]
Sensor fusion (best models)			
MAT+IMU	94.12 [92.56 95.68]	87.36 [82.67 92.05]	90.74 [87.95 93.53]
MAT+VID	92.58 [89.53 95.62]	90.27 [86.50 94.04]	91.42 [88.93 93.91]
IMU+VID	94.43 [92.53 96.34]	92.29 [89.59 94.99]	93.36 [91.75 94.97]
ALL 3-Nets	96.16 [95.03 97.29]	92.85 [90.23 95.46]	94.50 [93.05 95.95]
ALL 1-Net	92.87 [88.45 97.29]	93.60 [91.01 96.19]	93.24 [91.15 95.32]
Sens. – Sensitivity, Spec. – Specificity, BA – Balanced accuracy.			

The performance of the three-fold fusion (the combination of three networks; [ALL 3-Nets] considered) was superior to any of the single sensor alone (see Figure 4 and Tables 2 and 3). While the three-sensor fusion approach was also significantly better than the two-sensor fusions models where MAT was involved (i.e., MAT+IMU or MAT+VID), it was not superior to the combination of VID+IMU. Note, as reported above, although VID+IMU or VID+MAT was not significantly better than VID alone, combining all three modalities was superior than VID alone.

We also tested whether using features of all sensor modalities as input for one network (early fusion, ALL 1-Net) would lead to a better/worse classification accuracy as compared to the combination of three networks trained on the single sensor modalities (late fusion, ALL 3-Nets). While the average classification accuracy of the 3-Nets model (94.5%) was higher than that of the 1-Net model (93.2%), the difference was not statistically significant ( $p = 0.164$ ).

Table 3:  $p$ -values for the pairwise comparisons of the classification accuracies (balanced accuracy) of different models obtained from the Wilcoxon two-sided signed-rank test.

	IMU	VID	MAT+ IMU	MAT+ VID	IMU+ VID	ALL 3-Nets	ALL 1-Net
MAT	0.0547	0.0039**	0.0078**	0.0039**	0.0078**	0.0039**	0.0078**
IMU	-	0.9102	0.9102	1.0000	0.0078**	0.0039**	0.0078**
VID	-	-	1.0000	0.3594	0.0547	0.0117*	0.3008
MAT+IMU	-	-	-	0.4258	0.0742	0.0117*	0.0391*
MAT+VID	-	-	-	-	0.1289	0.0195*	0.3008
IMU+VID	-	-	-	-	-	0.2188	1.0000
ALL 3-Nets	-	-	-	-	-	-	0.1641

Asterisk symbols denote significant difference at the confidence level  $\alpha = 0.05$ : \* $p < 0.05$ , \*\* $p < 0.01$ .

## 4 Discussion

Following our experience in the use of mono-sensor approaches in the study of infant motor functions, we now propose a multimodal approach for movement recognition and classification. Using a fully synchronized multi-sensor dataset, in the present study we empirically tested and compared the utilities of three sensor modalities (pressure sensor, MAT; inertial sensors, IMU; and visual sensor, VID) and their various combinations (two- and three-sensor fusion approaches) for the same task. The task was to track and classify age-specific general movement patterns and differentiate between the absence or presence of a specific motor pattern during the first months of life, non-fidgety (FM-) vs. fidgety (FM+) movements, e.g., [47, 8, 9, 35, 34, 33].

To our first question, the performance of the single sensor modalities was different, with MAT (82.1%) being inferior to IMU (90.2%,  $p = 0.055$ ) and VID (90.7%,  $p < 0.01$ ). The performances of IMU and VID were, however, comparable, and also comparable to the average accuracy of divergent automated approaches for GMA studied to date, e.g., [7, 48, 15, 17, 18]. Nevertheless, these results were generated and validated on silo-data sets which do not allow for direct comparison of the findings.

The second methodological research question was whether sensor fusion improves classification accuracy. With the sensors available at the time of study conduct and used specifically for this task, the performance of the three-sensor fusion (94.5%) was significantly more accurate than any of the single modalities. It was also significantly superior than the two-sensor fusions of MAT+IMU (90.7%) or MAT+VID (91.4%). The average accuracy of the three-sensor fusion approach was again higher than the two-fold fusion of VID+IMU (93.4%), although the difference was not significant ( $p = 0.22$ ). The two-sensor fusion approaches with MAT (MAT+VID and MAT+IMU) were both significantly better than the performance of MAT alone; and the fusion with VID+IMU outperformed both MAT or IMU alone. With both two- and three-sensor fusions, the performances were superior than those of their single components, although some values were not statistically significant (Tables 2 and 3).

In our previous work, we extensively discussed possible reasons why MAT delivered moderate classification accuracy in our experiments, and the pros and cons of using divergent sensor modalities for infant motion tracking and classification [10]. With rapid technology advancement, the performance of each single modality (e.g., MAT) is likely to improve, which may further increase the accuracy of combined modalities (sensor fusion). This, however, needs to be tested in the future. For any specific task and with any single modality, the classification accuracy will eventually reach its limit (either ceiling or bottle neck). It is critical to examine, whether an approach with sensor fusion might be unnecessary (by perfect or ceiling accuracy of a single modality) or whether it is beneficial (by bottle neck of a single modality). If different dimensions of input (from diverse modalities) for the same phenomenon (e.g., motion) are augmented, the representation of the ground truth (e.g., distinguishable patterns) may be improved, hence increasing the overall classification accuracy, as shown in our current study. If, however, different modalities only provide redundant and highly correlated information in similar dimensions, then the combined approach may not outperform its single components.

As previously mentioned, all available automated GMA approaches solve only a fraction of

the tasks that are involved in a human GMA ([10]). This is legitimate and fundamental for the beginning of tool development, especially for proof-of-concept and method development endeavors. However, an AI tool, if intended to be used for real-time clinical practice, needs to go beyond providing dichotomous labels for a simplified task (e.g., FM+ or FM-), and with data from a limited sample. When more complicated tasks are demanded (e.g., divergent age-specific normal and inconspicuous movements vs. divergent age-inadequate or aberrant movements, each pointing to different clinical outcomes), it is important to evaluate again if a single modality method is sufficient, or, whether approaches with sensor fusion would be needed and generate rewarding results.

The third important question is whether sensor fusion approaches with non-intrusive modalities yield sufficient classification performance. Recall that GMA is not only valued for its efficiency and accuracy, but even more so for its convenience and non-intrusiveness to infants and their families. This is the reason why it has been widely accepted by families of divergent cultural backgrounds [49], and embedded in clinical routines. Note that a high number of infants in need of a GMA diagnosis are in poor or delicate health conditions. Attaching sensors to the infants' body is challenging, and, as known, could interfere with their behavioral states and hence their motor output (handbook; [38]). In a standard GMA, the assessor does not need to touch, manipulate or neurologically assess, but only observe the infant for a few minutes. If an automated solution aims to scale-up GMA in medical practice, it should maintain the non-intrusiveness and user-friendliness of the original method [8]. In this study, as presented above, the non-intrusive sensor fusion (MAT+VID) resulted in satisfying and significantly better accuracy (91.42%) than MAT alone (82.1%), and higher (yet not significant) accuracy than VID (90.7%). In other words, the fusion with non-intrusive sensors delivered promising results. We cannot tell at this point if the performance of MAT could be further improved (e.g., with refined technology customized for infant motion tracking), and whether the combined performance of MAT+VID would then change and surpass that of VID alone.

Notably, the pressure sensing mat is fully non-intrusive and effortless to install. It is also anonymous by nature, hence particularly suitable for acquiring and sharing multi-centered large-scaled clinical data in a short time, which may be the key for developing and advancing any data-driven AI approach [10]. That said, improving pressure sensing technology for infant motion tracking might be easier and faster than improving the technology of other sensing modalities. A single camera, as used in this study, is also non-intrusive and without complicated setups, and is a widely used and researched modality for automated GMA solutions [2, 1, 3]. However, compared to pressure sensors, cameras use implies confidentiality issues, which may hinder large scale data sharing. This must be circumvented (see [34] for an example) and is associated with additional costs and efforts. At present, applying intrusive wearable devices such as IMUs on the infant's body is still cumbersome and time-consuming. Still, future IMUs might be developed for effortless and user-friendly applications, which will make this sensing method more attractive. In our study, IMUs yielded a performance comparable to RGB cameras.

For developing the sensor-fusion method, we used a dataset of 1683 snippets from 45 infants, fully labelled by two human GMA assessors. The performances of the single sensor modalities and their combinations may be improved if larger datasets are used in future undertakings. Extended datasets would also allow the use of more advanced network architectures such as graph convolutional neural networks [15], spatio-temporal attention models [17], or spatial-temporal transformer models [7]. In addition, the utility of 3D skeletons instead of 2D skeletons [19, 7], or RGB-D sensors [19, 16], and the utility of ensemble classifiers [48, 15] may improve the classification performance of the fusion approach with non-intrusive sensors even further.

In our study, we compared two sensor fusion approaches: a combination of three networks trained on single sensor modalities vs. one network trained on all sensors (early vs. late sensor fusion; e.g., [50]). While on average classification accuracy of the late sensor fusion was slightly higher than that of the early fusion (94.5% and 93.2%, respectively), this difference in the classification performance was not statistically significant. However, we would argue that using the late sensor fusion approach (i.e., the combination of multiple networks) would be more advantageous. The first reason is that a modular approach (three separate networks) makes it easier to retrain or replace and retrain classifiers for the specific sensor modality. Feature space of single sensor modalities is much smaller as compared to the feature space of a combination of all the sensors. Larger feature spaces usually require larger networks, which leads to longer training time and may cause convergence issues. The other reason is that the single network would break down if during a multi-sensory recording one of the sensors failed (i.e., missing data from one sensor), since inputs

from all sensors are required for making predictions.

Last but not least, the sensor fusion approach currently needs complex setups and data analysis procedures as compared to single components, therefore it is associated with higher costs, greater efforts, and more technical requirements. If, however, the sensor fusion approach, especially the non-intrusive ones, could decisively improve the performance of automated solutions of GMA compared to that of the single modalities, the efforts would ultimately pay off. The sensor fusion approach is yet another attempt among many others developed over the past decades, aimed at generating automated GMA modalities with high accuracy and superior user experiences.

The multiple sensor fusion approach is a promising attempt for automating the classification of infant motor patterns. Complex evolving neurofunctions require equally complex (and very likely multi-sensor) assessments enabling a deeper understanding of infant development. We consider the multiple sensor fusion approach an essential methodological challenge towards realizing AI-based deep phenotyping and classification of infant movements. GMA studies and infant research over past decades suggest that age-specific endogenous movements are associated with different neurodevelopmental outcomes across distinct domains such as motor, social-communicative and cognitive functions [9, 51, 33, 52]. The multiple sensor fusion approach will add a novel and broader perspective to the prevailing single modality endeavors focusing on the recognition of a selected number of movement patterns, e.g., [7, 10, 27, 15, 28, 53, 2]. This work catalyzes further innovation, driving empirical studies to enable AI based solutions to effectively predict developmental trajectories associated with diverse outcomes.

## Data availability

The data will be made publicly available after acceptance of this manuscript.

## Code availability

The source code will be made publicly available after acceptance of this manuscript.

## References

- [1] M. T. Irshad, M. A. Nisar, P. Gouverneur, M. Rapp, and M. Grzegorzec, “AI approaches towards Prechtl’s assessment of general movements: A systematic literature review,” *Sensors*, vol. 20, no. 18, p. 5321, 2020.
- [2] N. Silva, D. Zhang, T. Kulvicius, A. Gail, C. Barreiros, S. Lindstaedt, M. Kraft, S. Bölte, L. Poustka, K. Nielsen-Saines, *et al.*, “The future of general movement assessment: The role of computer vision and machine learning – A scoping review,” *Research in Developmental Disabilities*, vol. 110, p. 103854, 2021.
- [3] K. Raghuram, S. Orlandi, P. Church, T. Chau, E. Uleryk, P. Pechlivanoglou, and V. Shah, “Automated movement recognition to predict motor impairment in high-risk infants: a systematic review of diagnostic test accuracy and meta-analysis,” *Developmental Medicine & Child Neurology*, vol. 63, no. 6, pp. 637–648, 2021.
- [4] M. Leo, G. M. Bernava, P. Carcagnì, and C. Distante, “Video-based automatic baby motion analysis for early neurological disorder diagnosis: State of the art and future directions,” *Sensors*, vol. 22, no. 3, p. 866, 2022.
- [5] Z. Peng, D. Kommers, R.-H. Liang, X. Long, W. Cottaar, H. Niemarkt, P. Andriessen, and C. van Pul, “Continuous sensing and quantification of body motion in infants: A systematic review,” *Heliyon*, vol. 9, no. 7, 2023.
- [6] L. Reinhart, A. C. Bischops, J.-L. Kerth, M. Hagemester, B. Heinrichs, S. Eickhoff, J. Dukart, K. Konrad, E. Mayatepek, and T. Meissner, “Artificial intelligence in child development monitoring: A systematic review on usage, outcomes and acceptance,” *Intelligence-based medicine*, p. 100134, 2024.
- [7] Q. Gao, S. Yao, Y. Tian, C. Zhang, T. Zhao, D. Wu, G. Yu, and H. Lu, “Automating general movements assessment with quantitative deep learning to facilitate early screening of cerebral palsy,” *Nature Communications*, vol. 14, no. 1, p. 8294, 2023.

- [8] H. F. R. Prechtl, C. Einspieler, G. Cioni, A. F. Bos, F. Ferrari, and D. Sontheimer, “An early marker for neurological deficits after perinatal brain lesions,” *The Lancet*, vol. 349, no. 9062, pp. 1361–1363, 1997.
- [9] I. Novak, C. Morgan, L. Adde, J. Blackman, R. N. Boyd, J. Brunstrom-Hernandez, G. Cioni, D. Damiano, J. Darrah, A.-C. Eliasson, *et al.*, “Early, accurate diagnosis and early intervention in cerebral palsy: Advances in diagnosis and treatment,” *JAMA Pediatrics*, vol. 171, no. 9, pp. 897–907, 2017.
- [10] T. Kulvicius, D. Zhang, K. Nielsen-Saines, S. Bölte, M. Kraft, C. Einspieler, L. Poustka, F. Wörgötter, and P. B. Marschik, “Infant movement classification through pressure distribution analysis,” *Communications Medicine*, vol. 3, no. 1, p. 112, 2023.
- [11] N. Sermpou and H. Gima, “Correlation between pose estimation features regarding movements towards the midline in early infancy,” *PLOS One*, vol. 19, no. 2, p. e0299758, 2024.
- [12] L. Letzkus, J. V. Pulido, A. Adeyemo, S. Baek, and S. Zanelli, “Machine learning approaches to evaluate infants’ general movements in the writhing stage – a pilot study,” *Scientific Reports*, vol. 14, no. 1, p. 4522, 2024.
- [13] S.-C. Lin, E. Chandra, P. N. Tsao, W.-C. Liao, W.-J. Chen, T.-A. Yen, J. Y.-J. Hsu, and S.-F. Jeng, “Application of artificial intelligence in infant movement classification: A reliability and validity study in infants who were full-term and preterm,” *Physical Therapy*, vol. 104, no. 2, p. pzad176, 2024.
- [14] A. Soualmi, O. Alata, C. Ducottet, H. Patural, and A. Giraud, “Mean 3D dispersion for automatic general movement assessment of preterm infants,” in *2023 45th Annual International Conference of the IEEE Engineering in Medicine & Biology Society (EMBC)*, pp. 1–5, IEEE, 2023.
- [15] D. Groos, L. Adde, S. Aubert, L. Boswell, R.-A. de Regnier, T. Fjortoft, D. Gaebler-Spira, A. Haukeland, M. Loennecken, M. Msall, U. I. Möinichen, A. Pascal, C. Peyton, H. Ramampiaro, M. D. Schreiber, I. E. Silberg, N. T. Songstad, N. Thomas, C. van den Broeck, G. K. Øberg, E. A. F. Ihlen, and R. Støen, “Development and validation of a deep learning method to predict cerebral palsy from spontaneous movements in infants at high risk,” *JAMA Network Open*, vol. 5, p. e2221325, 07 2022.
- [16] D. Balta, H. Kuo, J. Wang, I. G. Porco, O. Morozova, M. M. Schladen, A. Cereatti, P. S. Lum, and U. Della C., “Characterization of infants’ general movements using a commercial rgb-depth sensor and a deep neural network tracking processing tool: an exploratory study,” *Sensors*, vol. 22, no. 19, p. 7426, 2022.
- [17] B. Nguyen-Thai, V. Le, C. Morgan, N. Badawi, T. Tran, and S. Venkatesh, “A spatio-temporal attention-based model for infant movement assessment from videos,” *IEEE Journal of Biomedical and Health Informatics*, vol. 25, no. 10, pp. 3911–3920, 2021.
- [18] S. Reich, D. Zhang, T. Kulvicius, S. Bölte, K. Nielsen-Saines, F. B. Pokorny, R. Peharz, L. Poustka, F. Wörgötter, C. Einspieler, *et al.*, “Novel AI driven approach to classify infant motor functions,” *Scientific Reports*, vol. 11, no. 1, p. 9888, 2021.
- [19] K. D. McCay, E. S. L. Ho, D. Sakkos, W. L. Woo, C. Marcroft, P. Dulson, and N. D. Embleton, “Towards explainable abnormal infant movements identification: A body-part based prediction and visualisation framework,” in *IEEE EMBS International Conference on Biomedical and Health Informatics (BHI)*, pp. 1–4, 2021.
- [20] E. A. F. Ihlen, R. Støen, L. Boswell, R.-A. de Regnier, T. Fjortoft, D. Gaebler-Spira, C. Labori, M. C. Loennecken, M. E. Msall, U. I. Möinichen, *et al.*, “Machine learning of infant spontaneous movements for the early prediction of cerebral palsy: A multi-site cohort study,” *Journal of Clinical Medicine*, vol. 9, no. 1, p. 5, 2020.
- [21] T. Tsuji, S. Nakashima, H. Hayashi, Z. Soh, A. Furui, T. Shibanoki, K. Shima, and K. Shimatani, “Markerless measurement and evaluation of general movements in infants,” *Scientific Reports*, vol. 10, no. 1, p. 1422, 2020.
- [22] V. Marchi, V. Belmonti, F. Cecchi, M. Coluccini, P. Ghirri, A. Grassi, A. Sabatini, and A. Guzzetta, “Movement analysis in early infancy: Towards a motion biomarker of age,” *Early Human Development*, vol. 142, p. 104942, 2020.

- [23] D. Karch, K.-S. Kim, K. Wochner, J. Pietz, H. Dickhaus, and H. Philippi, “Quantification of the segmental kinematics of spontaneous infant movements,” *Journal of Biomechanics*, vol. 41, no. 13, pp. 2860–2867, 2008.
- [24] M. S. Abrishami, L. Nocera, M. Mert, I. A. Trujillo-Priego, S. Purushotham, C. Shahabi, and B. A. Smith, “Identification of developmental delay in infants using wearable sensors: Full-day leg movement statistical feature analysis,” *IEEE Journal of Translational Engineering in Health and Medicine*, vol. 7, pp. 1–7, 2019.
- [25] H. U. Chung, A. Y. Rwei, A. Hourlier-Fargette, S. Xu, K. Lee, E. C. Dunne, Z. Xie, C. Liu, A. Carlini, D. H. Kim, *et al.*, “Skin-interfaced biosensors for advanced wireless physiological monitoring in neonatal and pediatric intensive-care units,” *Nature Medicine*, vol. 26, no. 3, pp. 418–429, 2020.
- [26] M. Airaksinen, O. Räsänen, E. Ilén, T. Häyrynen, A. Kivi, V. Marchi, A. Gallen, S. Blom, A. Varhe, N. Kaartinen, *et al.*, “Automatic posture and movement tracking of infants with wearable movement sensors,” *Scientific Reports*, vol. 10, no. 1, p. 169, 2020.
- [27] M. Airaksinen, A. Gallen, A. Kivi, P. Vijayakrishnan, T. Häyrynen, E. Ilén, O. Räsänen, L. M. Haataja, and S. Vanhatalo, “Intelligent wearable allows out-of-the-lab tracking of developing motor abilities in infants,” *Communications Medicine*, vol. 2, no. 1, p. 69, 2022.
- [28] H. Jeong, S. S. Kwak, S. Sohn, J. Y. Lee, Y. J. Lee, M. K. O’Brien, Y. Park, R. Avila, J.-T. Kim, J.-Y. Yoo, *et al.*, “Miniaturized wireless, skin-integrated sensor networks for quantifying full-body movement behaviors and vital signs in infants,” *Proceedings of the National Academy of Sciences*, vol. 118, no. 43, p. e2104925118, 2021.
- [29] C. Fontana, V. Ottaviani, C. Veneroni, S. E. Sforza, N. Pesenti, F. Mosca, O. Picciolini, M. Fumagalli, and R. L. Dellacà, “An automated approach for general movement assessment: A pilot study,” *Frontiers in pediatrics*, p. 868, 2021.
- [30] D. den Hartog, M. M. van der Krogt, S. van der Burg, I. Aleo, J. Gijsbers, L. A. Bonouvrié, J. Harlaar, A. I. Buizer, and H. Haberfehlner, “Home-based measurements of dystonia in cerebral palsy using smartphone-coupled inertial sensor technology and machine learning: A proof-of-concept study,” *Sensors*, vol. 22, no. 12, p. 4386, 2022.
- [31] K. Kniaziew-Gomoluch, A. Szopa, Z. Kidoń, A. Siwiec, and M. Domagalska-Szopa, “Design and construct validity of a postural control test for pre-term infants,” *Diagnostics*, vol. 13, no. 1, p. 96, 2023.
- [32] K. Kniaziew-Gomoluch, A. Szopa, T. Łosień, J. Siwiec, Z. Kidoń, and M. Domagalska-Szopa, “Reliability and repeatability of a postural control test for preterm infants,” *International Journal of Environmental Research and Public Health*, vol. 20, no. 3, p. 1868, 2023.
- [33] C. Einspieler, R. Peharz, and P. B. Marschik, “Fidgety movements – tiny in appearance, but huge in impact,” *Jornal de Pediatria*, vol. 92, pp. 64–70, 2016.
- [34] P. B. Marschik, T. Kulvicius, S. Flügge, C. Widmann, K. Nielsen-Saines, M. Schulte-Rüther, B. Hüning, S. Bölte, L. Poustka, J. Sigafos, *et al.*, “Open video data sharing in developmental science and clinical practice,” *iScience*, vol. 26, no. 4, p. 106348, 2023.
- [35] P. B. Marschik, F. B. Pokorny, R. Peharz, D. Zhang, J. O’Muircheartaigh, H. Roeyers, S. Bölte, A. J. Spittle, B. Urlesberger, B. Schuller, *et al.*, “A novel way to measure and predict development: A heuristic approach to facilitate the early detection of neurodevelopmental disorders,” *Current Neurology and Neuroscience Reports*, vol. 17, no. 5, pp. 1–15, 2017.
- [36] A. Rihar, M. Mihelj, J. Pašič, G. Sgandurra, F. Cecchi, G. Cioni, P. Dario, and M. Munih, “Infant posture and movement analysis using a sensor-supported gym with toys,” *Medical & Biological Engineering & Computing*, vol. 57, pp. 427–439, 2019.
- [37] A. Rihar, M. Mihelj, J. Pašič, J. Kolar, and M. Munih, “Infant trunk posture and arm movement assessment using pressure mattress, inertial and magnetic measurement units (IMUs),” *Journal of Neuroengineering and Rehabilitation*, vol. 11, no. 1, pp. 1–14, 2014.
- [38] F. Ferrari, C. Einspieler, H. F. R. Prechtl, A. F. Bos, and G. Cioni, *Prechtl’s method on the qualitative assessment of general movements in preterm, term and young infants*. Mac Keith Press, 2004.
- [39] “Tekscan.” <https://www.tekscan.com/pressure-mapping-sensors>. Accessed: 2024-03-19.

- [40] “Xsens MTw Awinda.” <https://www.movella.com/products/wearables/xsens-mtw-awinda>. Accessed: 2024-03-19.
- [41] Y. Xu, J. Zhang, Q. Zhang, and D. Tao, “ViTPose: Simple vision transformer baselines for human pose estimation,” *Advances in Neural Information Processing Systems*, vol. 35, pp. 38571–38584, 2022.
- [42] Z. Cao, T. Simon, S.-E. Wei, and Y. Sheikh, “Realtime multi-person 2D pose estimation using part affinity fields,” in *IEEE Conference on Computer Vision and Pattern Recognition*, pp. 7291–7299, 2017.
- [43] Z. Cao, G. Hidalgo, T. Simon, S.-E. Wei, and Y. Sheikh, “OpenPose: Realtime multi-person 2D pose estimation using part affinity fields,” *IEEE Transactions on Pattern Analysis and Machine Intelligence*, vol. 43, no. 1, pp. 172–186, 2021.
- [44] “TensorFlow.” <https://www.tensorflow.org>. Accessed: 2024-03-21.
- [45] “Keras API.” <https://keras.io/api/>. Accessed: 2024-03-21.
- [46] “KerasTuner.” [https://keras.io/keras\\_tuner/](https://keras.io/keras_tuner/). Accessed: 2024-03-21.
- [47] C. Einspieler, P. B. Marschik, and H. F. R. Prechtel, “Human motor behavior: Prenatal origin and early postnatal development,” *Zeitschrift für Psychologie/Journal of Psychology*, vol. 216, no. 3, pp. 147–153, 2008.
- [48] K. D. McCay, P. Hu, H. P. H. Shum, W. L. Woo, C. Marcroft, N. D. Embleton, A. Munteanu, and E. S. L. Ho, “A pose-based feature fusion and classification framework for the early prediction of cerebral palsy in infants,” *IEEE Transactions on Neural Systems and Rehabilitation Engineering*, vol. 30, pp. 8–19, 2022.
- [49] C. Einspieler, A. F. Bos, A. J. Spittle, N. Bertocelli, M. Burger, C. Peyton, M. Toldo, F. Utsch, D. Zhang, and P. B. Marschik, “The general movement optimality score-revised (gmos-r) with socioeconomically stratified percentile ranks,” *Journal of Clinical Medicine*, vol. 13, no. 8, p. 2260, 2024.
- [50] K. Gadzicki, R. Khamsehashari, and C. Zetzsche, “Early vs late fusion in multimodal convolutional neural networks,” in *2020 IEEE 23rd international conference on information fusion (FUSION)*, pp. 1–6, IEEE, 2020.
- [51] C. Einspieler, A. F. Bos, M. E. Libertus, and P. B. Marschik, “The general movement assessment helps us to identify preterm infants at risk for cognitive dysfunction,” *Frontiers in Psychology*, vol. 7, p. 406, 2016.
- [52] Y. H. Lim, M. Licari, A. J. Spittle, R. E. Watkins, J. G. Zwicker, J. Downs, and A. Finlay-Jones, “Early motor function of children with autism spectrum disorder: a systematic review,” *Pediatrics*, vol. 147, no. 2, 2021.
- [53] Y. Khan and Z. Bao, “A soft-electronic sensor network tracks neuromotor development in infants,” *Proceedings of the National Academy of Sciences*, vol. 118, no. 46, p. e2116943118, 2021.

## Acknowledgments

The authors thank all families for their participation in this close-meshed prospective study. The initial idea of this study was conceptualized together with the “father of GMA”, Heinz Prechtel, and one of the leading experts in spontaneous infant movement assessment, Christa Einspieler. The transition from a Gestalt to an AI-based GMA would not have been possible without their guidance and skepticism on our initial ideas which was essential to develop the suggested methodology. Special thanks to the team members of the Marschik-Labs in Graz and Göttingen (iDN–interdisciplinary Developmental Neuroscience and SEE–Systemic Ethology and Developmental Science), who were involved in recruitment, accompanying families and their babies, data acquisition, data curation and pre-processing, and technical support: Gunter Vogrinec, Magdalena Krieger-Tomantschger, Iris Tomantschger, Laura Langmann, Claudia Zitta, Dr. Robert Peharz, Dr. Florian Pokorny, and Dr. Simon Reich. Special thanks also to our interdisciplinary international network of collaborators for discussing this study with us and for refining our views and ideas.

## **Author contributions**

Conceptualization, T.K., D.Z., and P.B.M.; Methodology, T.K., D.Z., F.W. and P.B.M; Data curation, T.K. and S.F.; Implementation and software, T.K.; Formal analysis, T.K. and D.Z.; Visualization, T.K.; Writing: Original draft, T.K., D.Z., F.W., and P.B.M.; Writing: Revision and editing, T.K., D.Z., L.P., S.B., L.J., M.K., M.Z., K.N., F.W. and P.B.M.; Supervision, F.W. and P.B.M.

## **Funding**

We are/were supported by Bio-TechMed Graz and the Deutsche Forschungsgemeinschaft (DFG – stand-alone grant 456967546, SFB1528 – project C03), the Bill and Melinda Gates Foundation through a Grand Challenges Explorations Award (OPP 1128871), the Volkswagen Foundation (project IDENTIFIED), the LeibnizScience Campus, the BMBF CP-Diadem (Germany), and the Austrian Science Fund (KLI811) for data acquisition, preparation, and analyses.

## **Competing interests**

The authors declare no competing interests.

# Supplementary information

## 1 Pre-processing of the video data

We denote position values for  $X$  and  $Y$  coordinates of the key points as  $x^p$  and  $y^p$ . Several pre-processing steps were performed as follows. First, to remove outliers (i.e., key points that were detected incorrectly) and to smooth the movement trajectories, we applied median and moving average filters with a sliding window size of 5 frames.

Then we centered body key points with respect to the average center point between the hip key points ( $h^c$ ) across all frames by:

$$h^c = \left[ \frac{1}{2n} \left( \sum_f x_f^{p_{10}} + \sum_f x_f^{p_{11}} \right), \frac{1}{2n} \left( \sum_f y_f^{p_{10}} + \sum_f y_f^{p_{11}} \right) \right],$$

$$x_f^{p_k} \leftarrow x_f^{p_k} - h_1^c, y_f^{p_k} \leftarrow y_f^{p_k} - h_2^c, \quad (2)$$

where  $k = 1 \dots 15$  is the key point index, and  $f = 1 \dots n$  ( $n = 250$ ) is the frame index.  $x_f^{p_{10,11}}$  and  $y_f^{p_{10,11}}$  correspond to the  $X$  and  $Y$  coordinates of the hip key points (see Figure 2a).

Afterwards, for each snippet we rotated the skeletons such that the middle line between the average hip and shoulder key points is aligned with the  $Y$  axis (see Figure 2a):

$$s^c = \left[ \frac{1}{2n} \left( \sum_f x_f^{p_4} + \sum_f x_f^{p_5} \right), \frac{1}{2n} \left( \sum_f y_f^{p_4} + \sum_f y_f^{p_5} \right) \right],$$

$$\alpha = \arccos (s^c \cdot [0 \ 1]^T / \|s^c\|), R = \begin{bmatrix} \cos(\alpha) & -\sin(\alpha) \\ \sin(\alpha) & \cos(\alpha) \end{bmatrix},$$

$$\begin{bmatrix} x_f^{p_k} \\ y_f^{p_k} \end{bmatrix} \leftarrow R \cdot \begin{bmatrix} x_f^{p_k} \\ y_f^{p_k} \end{bmatrix}, \quad (3)$$

where  $s^c$  is the average center point between shoulder key points,  $\alpha$  is the rotation angle, and  $R$  is the rotation matrix.  $x_f^{p_{4,5}}$  and  $y_f^{p_{4,5}}$  correspond to the  $X$  and  $Y$  coordinates of the shoulder key points (see Figure 2a).

Next, for each snippet we scaled size of the skeletons such that the body length between the hip and shoulder center points ( $h^c$  and  $s^c$ ) is equal to 1/3:

$$x_f^{p_k} \leftarrow \frac{x_f^{p_k}}{3|h_2^c - s_2^c|}, y_f^{p_k} \leftarrow \frac{y_f^{p_k}}{3|h_2^c - s_2^c|}. \quad (4)$$

Finally, for each snippet we centered the time series of each key point by subtracting the mean value of the corresponding time series.

In addition to the positions of the key points ( $x_f^{p_k}, x_f^{p_k}$ ), we also used their velocities ( $x_f^{v_k}, x_f^{v_k}$ ). Since the scale of velocity values is much smaller than the scale of position values, we normalized position and velocity values separately using z-score normalization. For this, we calculated mean and standard deviation values across all position (or velocity) time series in the training sets and then used these values to normalize the data in the training and test sets.

After pre-processing, and concatenation of position and velocity features, this led to the feature matrix of size  $250 \times 60$ :

$$\begin{bmatrix} x_1^{p_1} & y_1^{p_1} & \dots & x_1^{p_{15}} & y_1^{p_{15}} & x_1^{v_1} & y_1^{v_1} & \dots & x_1^{v_{15}} & y_1^{v_{15}} \\ x_2^{p_1} & y_2^{p_1} & \dots & x_2^{p_{15}} & y_2^{p_{15}} & x_2^{v_1} & y_2^{v_1} & \dots & x_2^{v_{15}} & y_2^{v_{15}} \\ \vdots & \vdots & \ddots & \vdots & \vdots & \vdots & \vdots & \ddots & \vdots & \vdots \\ x_n^{p_1} & y_n^{p_1} & \dots & x_n^{p_{15}} & y_n^{p_{15}} & x_n^{v_1} & y_n^{v_1} & \dots & x_n^{v_{15}} & y_n^{v_{15}} \end{bmatrix}, \quad (5)$$

with  $n = 250$  frames.

## 2 Pre-processing of the pressure mat data

We first cropped the area of size  $29 \times 26$  ([1:29, 4:29]) of the original grid size (see red rectangle in Figure 2b), since the sensor values outside this area were 0 in most of the cases. The cropped area contained 754 pressure sensor values. Generally, only two areas were strongly activated on the pressure mat (see Figure 2b). The activation at the top corresponds to the infants' shoulders and/or head, whereas activation at the bottom corresponds to the infant's hips. Thus, we split the cropped grid area of size  $29 \times 26$  into two parts,  $12 \times 26$  (top part) and  $17 \times 26$  (bottom part), and tracked the center of pressure (CoP) in these two areas.

Next, we computed position coordinates  $x^{t/b}$  and  $y^{t/b}$  of the CoP and the average pressure values  $p^{t/b}$  of the top ( $t$ ) and the bottom ( $b$ ) areas for each frame (we skip frame index for brevity):

$$x^{t/b} = \frac{\sum_{i,j} j \times p^{t/b}(i,j)}{\sum_{i,j} p^{t/b}(i,j)}, y^{t/b} = \frac{\sum_{i,j} i \times p^{t/b}(i,j)}{\sum_{i,j} p^{t/b}(i,j)}, p^{t/b} = \frac{\sum_{i,j} p^{t/b}(i,j)}{m^{t/b} \times n^{t/b}}, \quad (6)$$

where  $p^t(i,j)$  and  $p^b(i,j)$  correspond to the pressure sensor values at the position  $i,j$  ( $i = 1 \dots m^{t/b}, j = 1 \dots n^{t/b}$ ) of the top and bottom areas, respectively.

To reduce signal noise, for each time series  $x^{t/b}$ ,  $y^{t/b}$ , and  $p^{t/b}$ , we applied moving average filter with a sliding window size of 5 frames. To avoid biases that could be caused by infant's body size and weight, we normalized position and pressure values across top and bottom areas for each snippet between 0 and 1 as follows:

$$\begin{aligned} \gamma &= \max([\max(x^t) - \min(x^t), \max(y^t) - \min(y^t), \\ &\quad \max(x^b) - \min(x^b), \max(y^b) - \min(y^b)]), \\ x^{t/b} &\leftarrow \frac{x^{t/b} - \min(x^{t/b})}{\gamma}, y^{t/b} \leftarrow \frac{y^{t/b} - \min(y^{t/b})}{\gamma}, \end{aligned} \quad (7)$$

$$\begin{aligned} \beta &= \max([\max(p^t) - \min(p^t), \max(p^b) - \min(p^b)]), \\ p^{t/b} &\leftarrow \frac{p^{t/b} - \min(p^{t/b})}{\beta}. \end{aligned} \quad (8)$$

Finally, this led to the feature matrix of size  $500 \times 6$ :

$$\begin{bmatrix} x_1^t & y_1^t & p_1^t & x_1^b & y_1^b & p_1^b \\ x_2^t & y_2^t & p_2^t & x_2^b & y_2^b & p_2^b \\ \vdots & \vdots & \vdots & \vdots & \vdots & \vdots \\ x_n^t & y_n^t & p_n^t & x_n^b & y_n^b & p_n^b \end{bmatrix}, \quad (9)$$

with  $n = 500$  frames.

## 3 Pre-processing of the IMU data

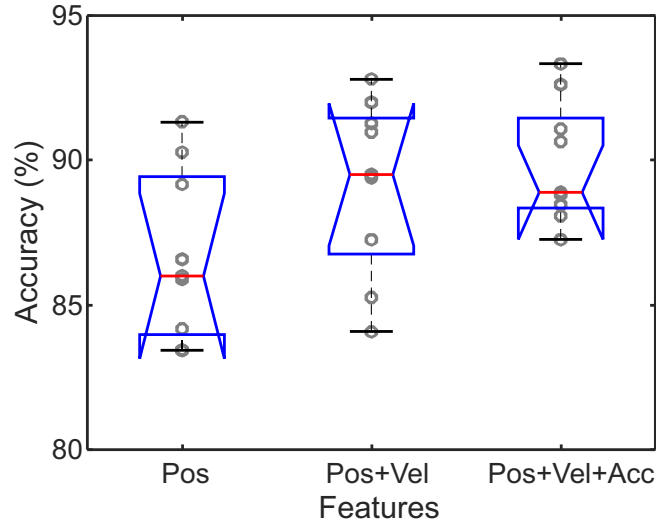
We denote accelerometer and gyrometer values as  $x^a, y^a, z^a$ , and  $x^g, y^g, z^g$ , respectively (see Figure 2c). We applied moving average filter for each sequence with a sliding window size of 5 frames, and then centered each time series by subtracting mean value of the corresponding time series.

The acceleration values and angular velocity values are of different scale, thus, we normalized acceleration values and angular velocity values separately using z-score normalization. For this, we calculated mean and standard deviation values across all acceleration (or angular velocity) time series in training sets and then used these values to normalize data in the training and test sets.

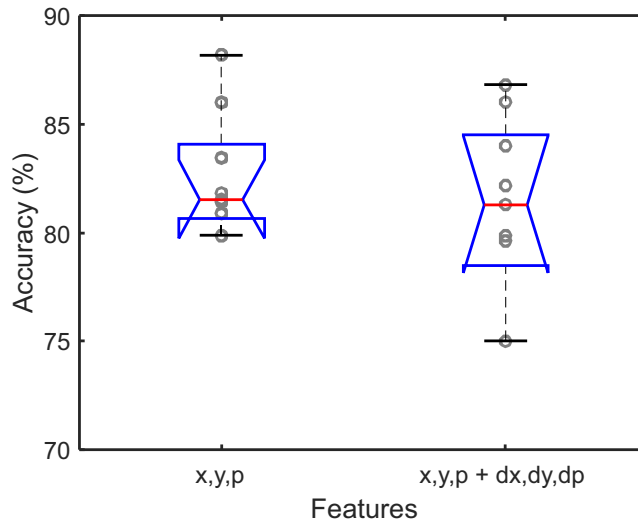
After pre-processing, and concatenation of acceleration and angular velocity values, this led to the feature matrix of size  $300 \times 36$ :

$$\begin{bmatrix} x_1^{a1} & y_1^{a1} & z_1^{a1} & x_1^{g1} & y_1^{g1} & z_1^{g1} & \dots & x_1^{a6} & y_1^{a6} & z_1^{a6} & x_1^{g6} & y_1^{g6} & z_1^{g6} \\ x_2^{a1} & y_2^{a1} & z_2^{a1} & x_2^{g1} & y_2^{g1} & z_2^{g1} & \dots & x_2^{a6} & y_2^{a6} & z_2^{a6} & x_2^{g6} & y_2^{g6} & z_2^{g6} \\ \vdots & \vdots & \vdots & \vdots & \vdots & \vdots & \ddots & \vdots & \vdots & \vdots & \vdots & \vdots & \vdots \\ x_n^{a1} & y_n^{a1} & z_n^{a1} & x_n^{g1} & y_n^{g1} & z_n^{g1} & \dots & x_n^{a6} & y_n^{a6} & z_n^{a6} & x_n^{g6} & y_n^{g6} & z_n^{g6} \end{bmatrix}, \quad (10)$$

with  $n = 300$  frames.



Supplementary Figure 1: Comparison of the classification accuracies on the test sets (9-fold cross-validation) using different skeleton features: only positions of the key points (Pos), positions and velocities of the key points (Pos+Vel), and positions, velocities and accelerations of the key points (Pos+Vel+Acc). We used CNN architecture with three convolutional layers (kernel parameters for each layer [numbers of kernels, filter size]: 8, 13x1; 32, 17x1; 64, 25x1) and one fully connected layer (256 units). Circles correspond to the classification accuracies for each fold. The box lines correspond to the lower quartile, median, and upper quartile values, and the whiskers represent ranges of the rest of the data. The notches represent a robust estimate of the uncertainty about the medians.



Supplementary Figure 2: Comparison of the classification accuracies on the test sets (9-fold cross-validation) using different pressure mat features: only  $x$ ,  $y$ ,  $p$  features, and  $x$ ,  $y$ ,  $p$  features and their first derivatives  $dx$ ,  $dy$ ,  $dp$ . We used CNN architecture with three convolutional layers (kernel parameters for each layer [numbers of kernels, filter size]: 8, 13x1; 32, 17x1; 64, 25x1) and one fully connected layer (256 units). Circles correspond to the classification accuracies for each fold. The box lines correspond to the lower quartile, median, and upper quartile values, and the whiskers represent ranges of the rest of the data. The notches represent a robust estimate of the uncertainty about the medians.

Supplementary Table 1: Parameter values for the hyperparameter tuning of the convolutional neural network architectures.

	Bayesian optimisation	Grid search (fine tuning)
Number of conv. layers	{1, 2, 3}	3
Number of kernels	Conv 1-3: {4, 8, 16, 32, 64, 128}	Conv 1: {4, 8} Conv 2: {8, 16, 32, 64} Conv 3: {8, 16, 32, 64}
Kernel size	Conv 1-3: {5×1, 7×1, 9×1, 13×1, 17×1, 25×1, 33×1}	Conv 1: {13×1, 17×1, 25×1} Conv 2: {7×1, 9×1, 13×1, 17×1, 25×1} Conv 3: {9×1, 13×1, 17×1, 25×1, 33×1}
Number of fully connect. (FC) layers	{1, 2}	1
Number of FC units	{64, 128, 256}	{128, 256}

Supplementary Table 2: Hyperparameters of the network architectures for different sensor modalities.

Model #	Input dim.	Convolutional layers (# of kernels, kernel size)			FC layer (# of units)	Out. dim.
		Conv 1	Conv 2	Conv 3	FC 1	
Pressure mat (MAT)						
1	500×6	8, 13×1	64, 17×1	16, 25×1	256	1
2		8, 13×1	32, 7×1	16, 33×1	128	
3		4, 17×1	64, 17×1	16, 13×1	128	
4		4, 17×1	16, 13×1	8, 33×1	128	
5		4, 17×1	64, 25×1	64, 17×1	256	
6		4, 17×1	32, 17×1	8, 13×1	128	
7		4, 17×1	8, 7×1	8, 33×1	128	
8		4, 13×1	16, 9×1	64, 33×1	256	
9		4, 25×1	32, 13×1	16, 13×1	256	
10		4, 17×1	64, 7×1	16, 9×1	128	
Inertial measurement units (IMU)						
1	300×36	8, 25×1	8, 17×1	64, 25×1	256	1
2		8, 25×1	64, 13×1	8, 25×1	256	
3		4, 13×1	64, 17×1	32, 33×1	128	
4		8, 17×1	8, 17×1	8, 17×1	128	
5		4, 17×1	64, 13×1	32, 33×1	128	
6		8, 25×1	32, 17×1	64, 33×1	128	
7		4, 25×1	32, 9×1	8, 9×1	128	
8		8, 25×1	8, 25×1	8, 33×1	128	
9		8, 25×1	32, 25×1	8, 33×1	128	
10		8, 17×1	64, 25×1	8, 13×1	128	
Video [skeleton] (VID)						
1	250×60	4, 13×1	32, 25×1	16, 25×1	128	1
2		4, 13×1	32, 17×1	64, 9×1	256	
3		8, 25×1	8, 13×1	64, 33×1	128	
4		4, 25×1	64, 7×1	32, 17×1	128	
5		4, 25×1	32, 25×1	16, 13×1	256	
6		4, 25×1	8, 25×1	64, 25×1	256	
7		4, 13×1	8, 7×1	64, 13×1	128	
8		8, 13×1	32, 13×1	64, 25×1	256	
9		8, 13×1	32, 7×1	64, 9×1	256	
10		4, 13×1	16, 25×1	64, 13×1	128	

Supplementary Table 3: Hyperparameters of the network architectures for the sensor fusion.

Model #	Input dim.	Convolutional layers (# of kernels, kernel size)			FC layer (# of units)	Out. dim.
		Conv 1	Conv 2	Conv 3	FC 1	
Sensor fusion (MAT+IMU+VID)						
1	250×102	4, 25×1	16, 7×1	64, 33×1	128	1
2		8, 13×1	8, 7×1	16, 25×1	256	
3		4, 25×1	32, 7×1	64, 33×1	256	
4		4, 13×1	16, 7×1	64, 17×1	128	
5		8, 17×1	64, 17×1	16, 17×1	256	
6		8, 25×1	8, 13×1	16, 13×1	256	
7		8, 17×1	8, 9×1	8, 9×1	256	
8		4, 17×1	64, 9×1	64, 25×1	256	
9		4, 13×1	16, 9×1	32, 9×1	256	
10		8, 17×1	8, 9×1	8, 17×1	256	

Supplementary Table 4: Classification results for the models trained on different sensor modalities. Average classification measures obtained from the 9-fold cross-validation together with confidence intervals of mean (CI 95%) are shown for each case. Models’ hyperparameters are specified in Supplementary Table 2.

Model #	Sens. (%) [ CI ]	Spec. (%) [ CI ]	BA (%) [ CI ]
Pressure mat (MAT)			
1	86.17 [82.78 89.55]	77.95 [69.68 86.22]	<b>82.06</b> [77.11 87.00]
2	86.84 [83.63 90.04]	74.71 [66.07 83.35]	80.77 [75.85 85.69]
3	84.77 [80.73 88.80]	76.28 [67.87 84.69]	80.53 [76.50 84.55]
4	86.18 [82.70 89.65]	73.95 [65.28 82.62]	80.06 [74.84 85.29]
5	86.10 [81.95 90.25]	72.75 [64.18 81.32]	79.43 [74.76 84.09]
6	86.05 [81.48 90.62]	72.28 [64.18 80.38]	79.17 [75.75 82.58]
7	86.64 [81.42 91.86]	71.10 [59.84 82.35]	78.87 [73.21 84.52]
8	87.03 [82.85 91.21]	69.41 [59.65 79.17]	78.22 [73.19 83.24]
9	85.54 [82.30 88.79]	69.59 [56.95 82.23]	77.57 [70.89 84.24]
10	87.91 [85.07 90.75]	66.88 [54.93 78.83]	77.39 [71.15 83.64]
Inertial measurement units (IMU)			
1	92.91 [90.28 95.55]	87.52 [83.47 91.57]	<b>90.22</b> [87.61 92.82]
2	93.30 [89.96 96.64]	86.75 [81.38 92.12]	90.02 [87.18 92.87]
3	94.92 [92.51 97.33]	85.03 [80.30 89.75]	89.97 [87.47 92.47]
4	91.48 [88.95 94.02]	87.70 [81.30 94.10]	89.59 [86.06 93.12]
5	91.86 [89.15 94.56]	86.06 [77.25 94.86]	88.96 [84.94 92.97]
6	91.11 [85.72 96.49]	85.75 [77.64 93.85]	88.43 [83.63 93.22]
7	91.53 [88.54 94.53]	85.30 [81.22 89.39]	88.42 [85.35 91.49]
8	91.18 [86.56 95.79]	85.49 [78.11 92.86]	88.33 [84.60 92.06]
9	90.80 [85.35 96.25]	84.78 [79.82 89.74]	87.79 [84.43 91.15]
10	90.62 [86.98 94.26]	84.45 [79.33 89.57]	87.54 [84.20 90.87]
Video [skeleton] (VID)			
1	91.67 [89.80 93.55]	89.65 [85.89 93.41]	<b>90.66</b> [88.91 92.41]
2	90.57 [87.33 93.81]	90.45 [85.23 95.68]	90.51 [88.02 93.00]
3	90.97 [88.72 93.23]	87.90 [83.88 91.92]	89.44 [87.22 91.65]
4	92.57 [90.85 94.28]	86.15 [81.28 91.02]	89.36 [87.33 91.38]
5	92.35 [89.93 94.77]	84.80 [80.01 89.58]	88.57 [86.42 90.73]
6	89.17 [86.06 92.28]	87.40 [82.70 92.09]	88.28 [86.23 90.34]
7	90.47 [89.11 91.84]	85.97 [79.62 92.33]	88.22 [85.42 91.02]
8	91.03 [88.89 93.17]	85.20 [78.90 91.50]	88.12 [85.09 91.15]
9	90.15 [87.70 92.61]	86.07 [79.60 92.55]	88.11 [85.65 90.58]
10	91.09 [88.30 93.88]	84.53 [77.72 91.35]	87.81 [85.25 90.37]
Sens. – Sensitivity, Spec. – Specificity, BA – Balanced accuracy.			
Numbers in bold font correspond to the highest classification accuracy for the specific sensor modality.			

Supplementary Table 5: Classification results for the models trained on the combination of all sensor modalities. Average classification measures obtained from the 9-fold cross-validation together with confidence intervals of mean (CI 95%) are shown for each case. Model parameters are specified in Supplementary Table 3.

Model #	Sens. (%) [ CI ]	Spec. (%) [ CI ]	BA (%) [ CI ]
Sensor fusion (MAT+IMU+VID)			
1	92.87 [88.45 97.29]	93.60 [91.01 96.19]	<b>93.24</b> [91.15 95.32]
2	94.32 [90.81 97.84]	90.39 [86.20 94.57]	92.36 [90.92 93.80]
3	92.87 [88.67 97.06]	90.78 [86.14 95.41]	91.82 [89.55 94.09]
4	94.22 [91.45 96.98]	89.40 [84.45 94.36]	91.81 [89.62 94.00]
5	93.03 [89.12 96.93]	90.02 [85.31 94.73]	91.52 [89.46 93.59]
6	93.31 [89.16 97.46]	89.26 [82.29 96.22]	91.28 [88.10 94.47]
7	91.84 [88.59 95.09]	90.52 [84.96 96.07]	91.18 [88.41 93.95]
8	92.48 [88.95 96.01]	86.92 [79.33 94.51]	89.70 [85.89 93.50]
9	91.86 [88.28 95.43]	89.94 [84.70 95.18]	90.90 [87.73 94.06]
10	91.61 [87.09 96.12]	89.47 [83.52 95.42]	90.54 [87.62 93.45]
Sens. – Sensitivity, Spec. – Specificity, BA – Balanced accuracy.			
The number in bold font corresponds to the highest classification accuracy.			